Neutron/gamma discrimination and localization with pixelated plastic scintillators and SiPM dedicated multiplexing readout

Clement Lynde, Camille Frangville, Aya Kanj, Romuald Woo, Vincent Schoepff, Guillaume Bertrand, Jean-Michel Bourbotte, Matthieu Hamel, Jonathan Dumazert, Frédérick Carrel

▶ **To cite this version:**

Clement Lynde, Camille Frangville, Aya Kanj, Romuald Woo, Vincent Schoepff, et al.. Neutron/gamma discrimination and localization with pixelated plastic scintillators and SiPM dedicated multiplexing readout. NDIP20 - 9th Conference on new develpment in photodetection, Jul 2022, Troyes, France. cea-04216662

HAL Id: cea-04216662
https://cea.hal.science/cea-04216662

Submitted on 25 Sep 2023

HAL is a multi-disciplinary open access archive for the deposit and dissemination of scientific research documents, whether they are published or not. The documents may come from teaching and research institutions in France or abroad, or from public or private research centers.

L'archive ouverte pluridisciplinaire **HAL**, est destinée au dépôt et à la diffusion de documents scientifiques de niveau recherche, publiés ou non, émanant des établissements d'enseignement et de recherche français ou étrangers, des laboratoires publics ou privés.

Neutron/gamma discrimination and localization with pixelated plastic scintillators and SiPM dedicated multiplexing readout

C. Lynde[1], C. Frangville[1], R. Woo[1], V. Schoepff[1], G. H. V. Bertrand[1], J.-M. Bourbotte[1], M. Hamel[1], J. Dumazert[1], F. Carrel[1]

[1] *Université Paris-Saclay, CEA, List, F-91120, Palaiseau, France*

I. Materials and Methods

A. SiPM array and plastic scintillators

The dimensions of all manufactured plastic scintillators (PSs) were chosen to match those of the ArrayC-30035-16P SiPM from SensL [1]. The PS #1.1 and #1.2, (Fig. 1) were monolithic and composed of chemicals allowing the discrimination of fast neutrons from gamma rays [2]. PS #1.1 (left in Fig. 1) was 12×12×10 mm^3 and covered by Teflon® for the measurement (middle in Fig. 1). PS #1.2 (right in Fig. 1) was a resized version of PS #1.1 where the thickness was reduced to 3 mm.

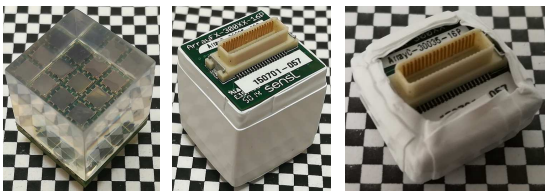

Fig. 1: Monolithic PS. Left: uncovered PS #1.1. Middle: Teflon® covered PS #1.1. Right: Teflon® covered PS #1.2.

Two approaches were attempted to manufacture pixelated PS. The chemical composition used for those PSs was a previously reported ^{6}Li-doped PS with fast/thermal neutron and gamma ray discrimination capabilities [3]. The first approach was based on a mechanical fabrication of small distinct pixels obtained from a monolithic PS. Each pixel was cut, polished and assembled to form the desired matrix, PS #2.1, #2.2 and #2.3, as showed in Fig. 2.

Fig. 2: Pixelated PS. Left: 1×1 PS #2.1. Middle: 2×2 PS #2.2. Right: 4×4 PS #2.3.

The second approach involved a direct polymerization of PS inside an *ad hoc* Teflon® mold. Therefore the mold was designed in order to precisely fit the SiPM detection cells, such as each pixelated PS has dimensions of 3×3×3 mm^3. 1 mm of Teflon® was used to separate the light response of each pixel. A digital model of the mold was made on SolidWorks® (left in Fig. 3) and several mold batches were machined (middle of Fig. 3). Finally, the mold was added at the bottom of a glass vial filled with a previously degassed solution of monomers and fluorophores (typically 72.8%$_{wt}$ Styrene, 8.09%$_{wt}$ Methacrylic Acid, 2.43%$_{wt}$ ^{enriched}Li-α-valerate, 16.66%$_{wt}$ PPO, 0.02%$_{wt}$ POPOP). The bottle was then sealed under an argon atmosphere before a thermally initiated polymerization took place for curing temperatures between 60 – 110°C. PS #3 was then obtained by cutting the excess of scintillating plastic and polish.

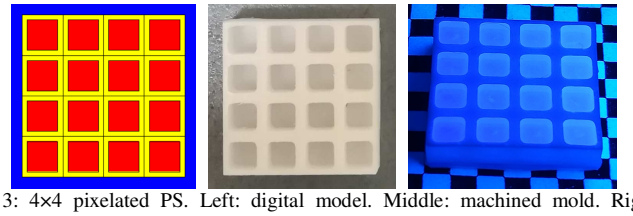

Fig. 3: 4×4 pixelated PS. Left: digital model. Middle: machined mold. Right: manufactured 4×4 PS #3.

B. Diode coupled symmetric charge division readout

In order to minimize the number of channels to be digitized, we used a multiplexing readout from AiT [4], [5], which reduced the 16-channels input to four "position" signals and one "sum" signal. This readout implements a diode coupled symmetric charge division (DCSCD) circuit dedicated to SiPM. It was originally developed for nuclear medicine imagers, where SiPM replace PMT and the scintillators used are an inorganic crystal. To the best of our knowledge, it has never been tested on organic scintillators. With a modular approach, AiT has decomposed the overall acquisition chain into three boards (Fig. 5). The "amplifier board power supply" (ABPS) provides the bias voltage for the SiPM and the +5V and -5V voltages for the amplifiers. The "4-channel active base" (AB4) encodes the SiPM signals into four encoded position signals. The "4-channel active base receiver" (ABR4) interconnects the ABPS and the AB4 and sums the four encoded signals. The measurements of the five signals were performed with a CAEN "DT5743" digitizer at 400 mega-samples/s.

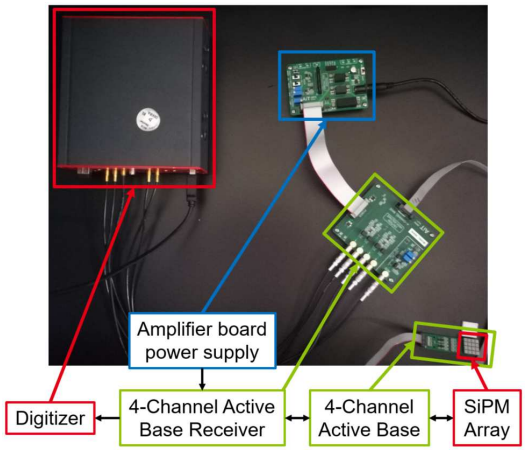

Fig. 5: Acquisition chain with the multiplexing readout from AiT.

C. Signal processing

The DCSCD circuit is based on the row/column readout of the Symmetric Charge Division (SCD) circuit [6]. When a particle generates a pulse of light collected by a SiPM, a unique combination of weights is applied to the induced electrical signal and divided the latter into two X (X^+ and X^-) and two Y (Y^+ and Y^-) signals. Since each combination of weights corresponds to a particular position, an algorithm similar to Anger logic [7] was used to decode the position of the original signal.

The pulse shape discrimination (PSD) principle used in this work is the charge comparison method (CCM) [8]. This method was applied to the "sum" signal and is based on ratios of pulse integrals over two different time periods optimized with the procedure proposed in [9].

II. Results and Discussion

A. Spatial response

The first tests were performed with the monolithic PS #1.1 (left in Fig. 6). We found the results to be inconclusive because the light was homogeneously distributed over the SiPM matrix, either due to the scintillator thickness or its non-pixelated state. The results with

the PS #1.2 (right in Fig. 6) showed that the reduction in thickness was not sufficient.

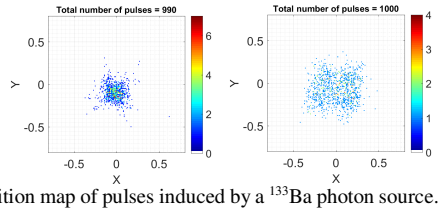

Fig. 6: 2-D position map of pulses induced by a ^{133}Ba photon source. Left: within the PS #P1.1. Right: within the PS #P1.2.

On the other hand, tests carried out with pixelated PS were significantly more conclusive. In Fig. 7, the 2-D map of the positions calculated from the signals is representative of the number and positioning of the scintillators on the SiPM matrix. One can clearly distinguish the pixelization of the detection. In contrast, it can be observed on the right image in Fig. 7 that the counting is not evenly distributed in the image for the assembled PS #2.3, whereas it is definitely more consistent with the molded PS #3 (Fig. 8). We explain this inhomogeneity mainly due to the non-uniformity of the SiPM gain factor within the array, and to a lesser extent of the PS pixel light yield. These results remained extremely promising and could be corrected by using an equalization matrix.

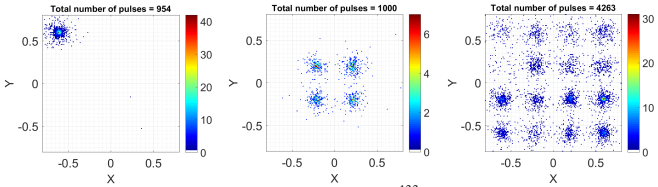

Fig. 7: 2-D position map of pulses induced by a ^{133}Ba source. Left: within the PS #P2.1. Middle: within the PS #P2.2. Right: within the PS #P2.3.

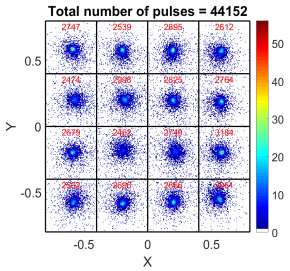

Fig. 8: 2-D position map of pulses induced by a ^{133}Ba source within the PS #3.

B. Energy response

Spectral measurements were performed with ^{22}Na and ^{137}Cs sources, and are presented in Fig. 9. The Compton edges of ^{22}Na at 341 keV and 1062 keV, and of ^{137}Cs at 477 keV, were not assessable when the whole matrix ("_Full" solid lines in Fig. 9) was measured. However, they started to become visible when only one pixel ("_Mono" dotted lines in Fig. 9) was measured. These results confirmed that the non-uniformity of the SiPM gain factor is of great importance. A first approximate calibration was nevertheless carried out based on these spectra.

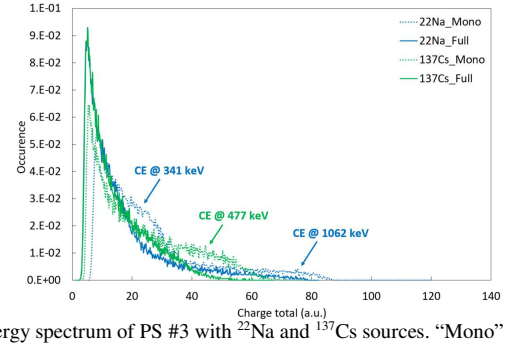

Fig. 9: Energy spectrum of PS #3 with ^{22}Na and ^{137}Cs sources. “Mono” corresponds to one pixel of the PS and “Full” to the full matrix.

C. Triple fast/thermal neutron and gamma discrimination

To illustrate the possibility to assess the triple discrimination with the pixelated PS #3, the classical biparametric histogram was obtained with a non-thermalized (left of Fig. 10) and thermalized (left of Fig. 10) ^{252}Cf source. The results showed the appearance of an ovoid area caused by the ions generated after the capture of a thermal neutron by a ^{6}Li nucleus. For an energy range above around 250 keVee, these results thereby exhibits a first triple discrimination of n_{th}/n_{fast}/gamma reached with a pixelated PS coupled on SiPM arrays for a FoM at 0.90.

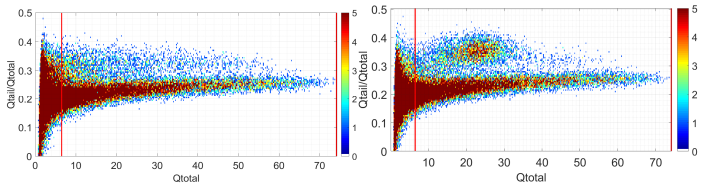

Fig. 10: Biparametric histogram of tail-to-total integral as a function of the total integral obtained with a ^{252}Cf source. Top: non-thermalized. Bottom: thermalized.

D. Neutron detection efficiency

The neutron detection efficiency was experimentally evaluated for PS #3. After applying gamma/neutron discrimination by the CCM, the neutron detection efficiency was calculated and compared to simulation in Table 1. The intrinsic efficiency corresponds to the ratio of the number of counts by the number of impinging neutrons through the detector. The extrinsic efficiency is defined as the ratio of the number of counts by the number of neutrons emitted by the source. The simulated and experimental source was a ^{252}Cf isotropic source placed at 15 cm from the surface of the detector. An extrinsic neutron detection efficiency of 1.97×10^{-6} was measured and intrinsic of 3.86×10^{-3}. Based on the simulated results, it was expected that the neutron detection efficiency would be four times higher. We explain this difference by the fact that the energy threshold applied in the simulations is not the same as that of the measurements.

Table 1: Comparison of neutron detection efficiency between simulations and experiments with the PS #3.

PS #3	Neutron detection efficiency	
	Intrinsic	Extrinsic
Simulation	1.50×10^{-2}	7.65×10^{-6}
Experimental	3.86×10^{-3}	1.97×10^{-6}

III. Conclusions and Future Work

In this study, the use of a multiplexing readout dedicated to SiPM was applied to pixelated plastic scintillators for gamma/neutron discrimination and localization. The first experimental results confirmed the possibility of simultaneously acquiring the position of an interaction and classifying it according to the type of particles in a 4×4 matrix of 3×3×3 mm^3 plastic scintillators. Next experimental studies will include the measurement of the intrinsic gain of SiPMs and their temperature dependence in order to equalize the response within the array. Further characterizations should allow an optimization of the position-sensitive neutron detector. Homogenization of the gain with correcting factors should lead to a better energy calibration, spatial resolution and uniformity, gamma and neutron sensitivity and discrimination.

Future work will focus on two main points: the pixelated PS scale up and the signals readout (hardware and software). We intend to increase the area and thickness of the detector as well as its pixelization; and to develop a miniaturized electronic readout with embedded data processing.

REFERENCES

[1] SensL, "C-series Low Noise, Blue-Sensitive Silicon Photomultipliers datasheet." pp. 1–17, 2016.

[2] G. H. V. Bertrand, M. Hamel, S. Normand, and F. Sguerra, "Pulse shape discrimination between (fast or thermal) neutrons and gamma rays with plastic scintillators: State of the art," *Nucl. Instruments Methods Phys. Res. Sect. A Accel. Spectrometers, Detect. Assoc. Equip.*, vol. 776, pp. 114–128, 2015, doi: 10.1016/j.nima.2014.12.024.

[3] C. Frangville, M. Hamel, G. H. V. Bertrand, E. Montbarbon, A. Grabowski, and C. Lynde, "Large solubility of lithium carboxylates reaching high rates of 6Li incorporation in polystyrene-based plastic scintillators for fast/thermal neutron and gamma ray detection," *Mater. Chem. Front.*, vol. 3, no. 8, pp. 1626–1631, 2019.

[4] James Proffitt, "Diode enhanced amplifier circuits and methods thereof," 2013.

[5] S. Majewski, J. Proffitt, A. Stolin, and R. Raylman, "Development of a 'resistive' readout for SiPM arrays," *IEEE Nucl. Sci. Symp. Conf. Rec.*, vol. 9059, pp. 3939–3944, 2011, doi: 10.1109/NSSMIC.2011.6153749.

[6] V. Popov, S. Majewski, and A. G. Weisenberger, "Readout electronics for multianode photomultiplier tubes with pad matrix anode layout," *IEEE Nucl. Sci. Symp. Conf. Rec.*, vol. 3, pp. 2156–2159, 2003, doi: 10.1109/nssmic.2003.1352307.

[7] H. O. Anger, "Scintillation camera," *Rev. Sci. Instrum.*, vol. 29, pp. 27–33, 1958.

[8] D. Wolski, M. Moszyński, T. Ludziejewski, A. Johnson, W. Klamra, and Ö. Skeppstedt, "Comparison of n-γ discrimination by zero-crossing and digital charge comparison methods," *Nucl. Instruments Methods Phys. Res. Sect. A Accel. Spectrometers, Detect. Assoc. Equip.*, vol. 360, no. 3, pp. 584–592, 1995.

[9] C. Lynde *et al.*, "Optimization of the charge comparison method for multi-radiation field using various measurement systems," *IEEE Trans. Nucl. Sci.*, vol. 9499, no. c, pp. 1–9, 2020, doi: 10.1109/TNS.2020.2966886.